A water-based synthetic route to metal-organic framework UiO-66 starting from PET-derived terephthalate esters

Pietro Agola[a] and Marco Taddei[a,b*]

[a] *Department of Chemistry and Industrial Chemistry, INSTM research unit, University of Pisa, Via G. Moruzzi 13, 56124 Pisa, Italy.*

[b] *Centro per l'Integrazione della Strumentazione scientifica dell'Università di Pisa (C.I.S.U.P.), Università di Pisa, 56124 Pisa, Italy*

ELECTRONIC SUPPLEMENTARY INFORMATION

Preliminary synthetic screening

Table S1. Results of preliminary screening using 1 mmol DMT and 1 mmol $ZrOCl{\cdot}8H_2O$ in 10 mL total volume. Workup protocol: 10 mL 0.1 M TEA in MeOH, 60 min x 2; 10 mL MeOH, 60 min x 2; 10 mL acetone, 60 min x 1.

Sample	Temperature (°C)	HCl (eq)	AA (eq)	Time (h)	RME[a] (%)	Phase	FWHM[b] (°)
P1	80	10	10	24	34	**hcp**	0.29
P2	90	10	10	24	40	**hcp**	0.25
P3	130	10	10	24	13	**hcp**	-[c]
P4	90	10	0	24	50	**hcp** + H_2BDC	-[d]
P5	80	20	20	24	16	**fcu/reo** + H_2BDC	-[d]
P6	90	20	20	5	20	**fcu/reo**	0.16
P7	100	20	20	5	10	**fcu/reo**	0.17
P8	90	20	10	24	35	**hcp**	0.32
P9	90	20	20	24	23	**fcu/reo**	0.17

[a] Maximum RME obtainable starting from DMT and assuming an ideal defect free product with **fcu** topology of formula $Zr_6O_4(OH)_4(BDC)_6$ = 54%. Maximum RME obtainable starting from DMT and assuming a product with **hcp** topology of formula $Zr_{12}O_8(OH)_{14}(BDC)_9$ = 47%; [b] FWHM of reflection 111 for **fcu** phase and reflection 101 for **hcp** phase (both reflections are located at 7.3°); [c] the 101 reflection is superimposed with the 100 reflection; [d] FWHM not reported for mixed phase systems.

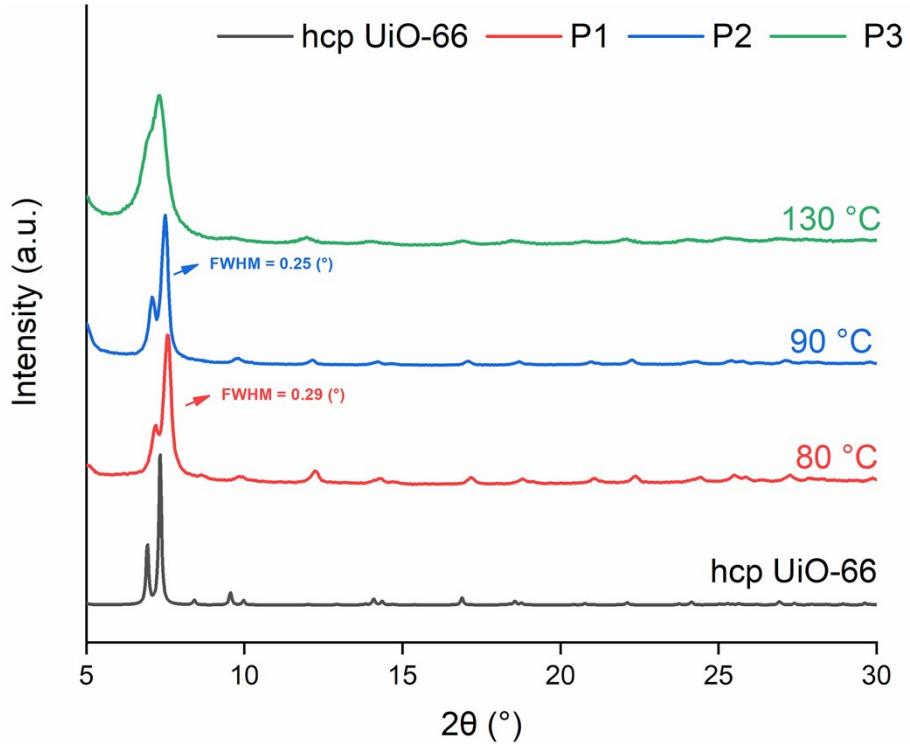

Figure S1. PXRD patterns of P1 (red, 80 °C), P2 (blue, 90 °C), P3 (green, 130 °C), compared to the calculated pattern for **hcp** UiO-66 (black). Reaction conditions: 10 eq AA, 10 eq HCl, 24 h.

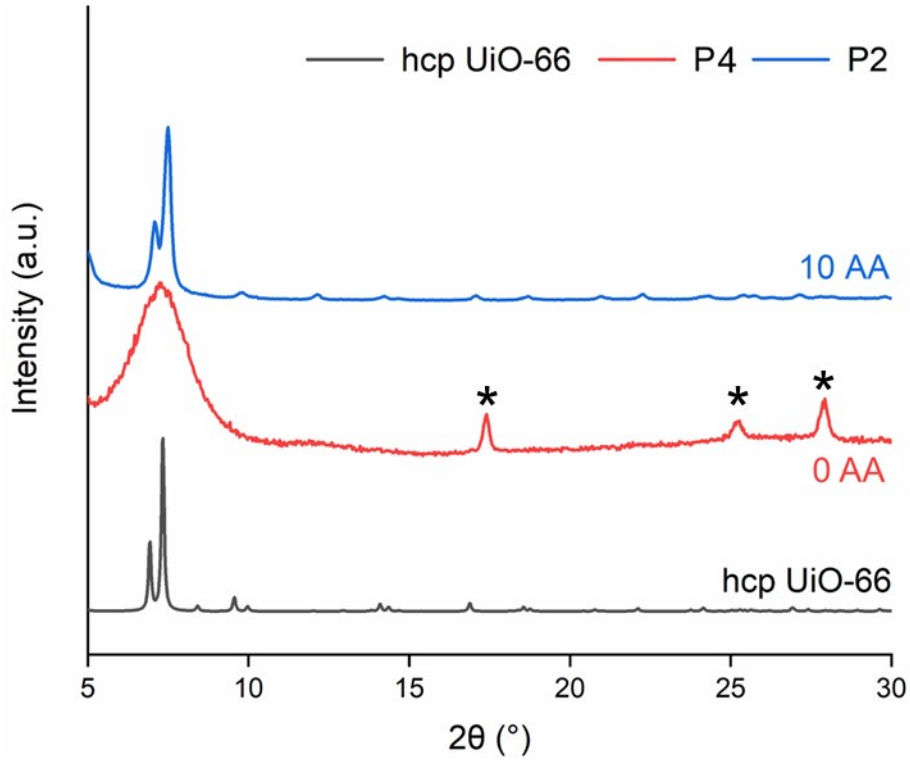

Figure S2. PXRD patterns of P4 (red, 0 eq AA) and P2 (blue, 10 eq AA). Reaction conditions: 10 HCl, 24 h, 90 °C. Asterisks (*) indicate peaks associated with crystallised H_2BDC in P4.

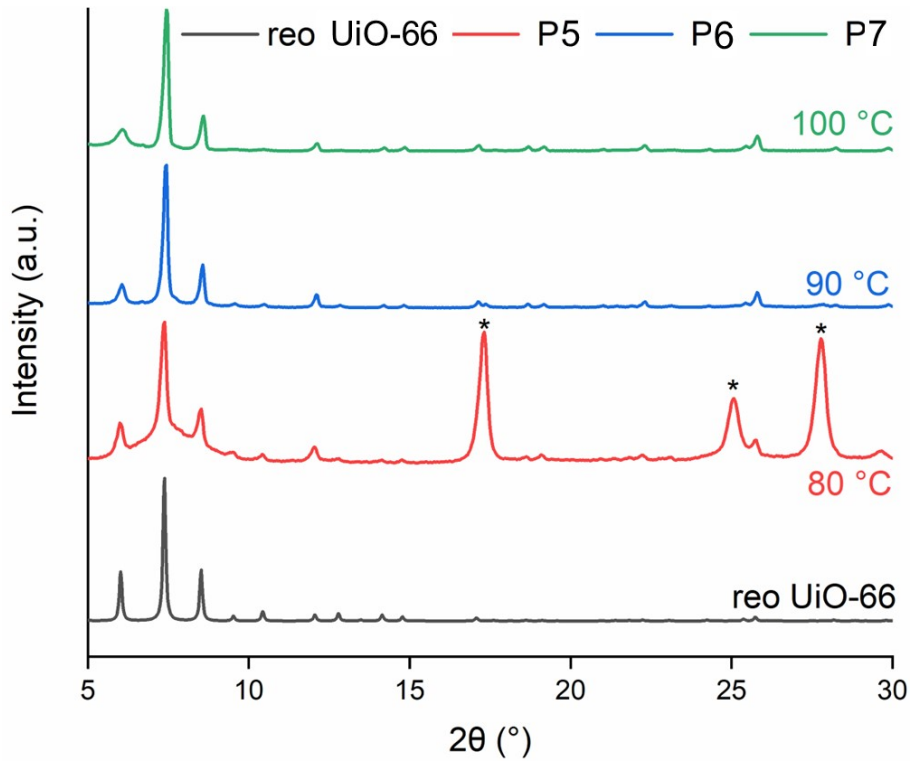

Figure S3. PXRD patterns of P5 (red, 80 °C), P6 (blue, 90 °C) and P7 (green, 100 °C). Reaction conditions: 20 eq AA, 20 eq HCl. Asterisks (*) indicate peaks associated with crystallised H_2BDC in P5.

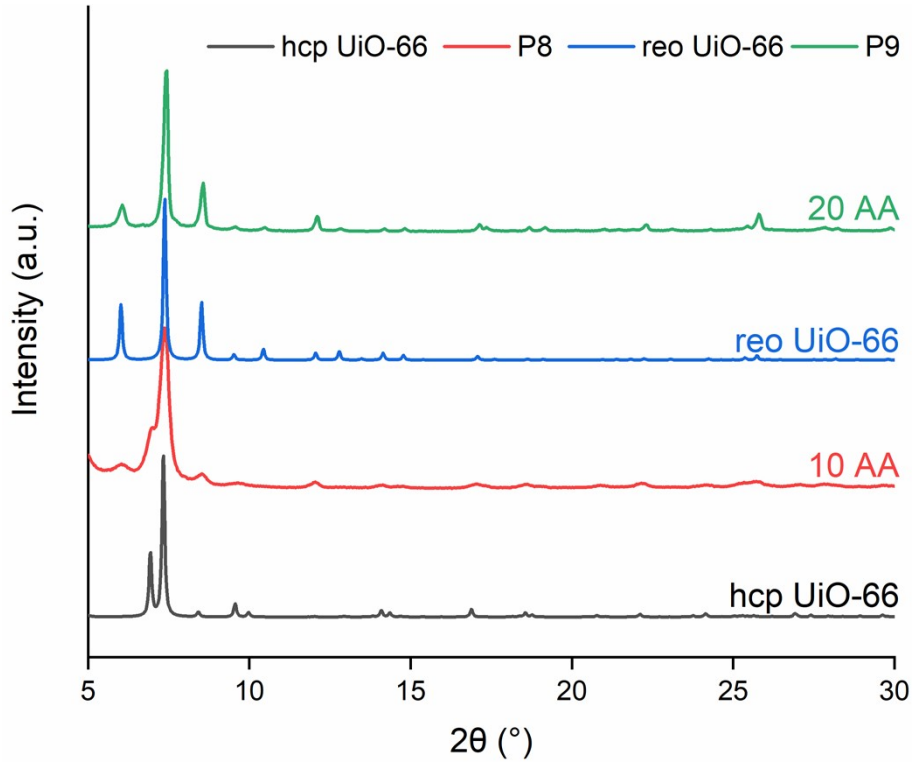

Figure S4: PXRD patterns of P8 (red) and P9 (blue). Reaction conditions: 20 eq HCl, 24 h, 90 °C.

Mechanistic hypothesis

Table S2: syntheses performed starting from 1 mmol H_2BDC and 1 mmol $ZrOCl{\cdot}8H_2O$ in aqueous medium (10 mL total volume).

Sample	Temperature (°C)	HCl (eq)	AA (eq)	Time (h)	RME (%)
P10	100	20	20	24	no product
P11	90	-	10	24	no product
P12	90	-	-	5	no product

With P10, the objective was to evaluate the formation of solid product working in similar conditions to those of the previously described experiments, simply using H_2BDC instead of DMT. After washing the product with DMF, it was noted that it completely dissolved, suggesting that the obtained white solid was unreacted H_2BDC. It was hypothesized that, because of the presence of HCl, H_2BDC remains protonated and cannot coordinate to zirconium. Based on this hypothesis, P11 was conducted in the absence of HCl and with a lower content of AA (10 eq). Despite these precautions, also in this case no formation of the MOF was observed. To verify if the presence of AA was responsible for no MOF formation, P12 was conducted in the absence of either acid. Also in this test, the result was the same, with H_2BDC as the only end solid product.

Table S3: syntheses performed starting from 1 mmol H_2BDC and 1 mmol $ZrOCl{\cdot}8H_2O$ in methanolic medium (10 mL total volume).

Sample	Temperature (°C)	HCl (eq)	H_2O[a] (eq)	Time (h)	RME (%)	Phase	FWHM[c] (°)
P13	RT	20	80	168	7	-[d]	-[d]
P14	60	20	80	24	60	**fcu**	0.40
P15	60	30	114	96	54	**fcu**	0.41
P16	90	20	80	24	51	**fcu**	0.47

[a] Water originating from the HCl solution (37 wt% in water, 12 M); [b] Maximum RME obtainable starting from H_2BDC and assuming an ideal defect free product with **fcu** topology of formula $Zr_6O_4(OH)_4(BDC)_6$ = 57%; [c] FWHM of reflection 111 (located at 7.3°); [d] nearly amorphous product

All reactions in Table S3, except for P13, show high RME. This difference can be attributed to the lower temperature of P13, that may have kinetically hampered the reaction. From the comparison of P14, P15 and P16, it seems that higher temperatures or higher concentration of HCl lead to a slight decrease in RME. **Figure S5** shows that all the three samples are **fcu** UiO-66. It seems that this type of synthesis is very robust since there are no significant differences in diffraction patterns with changes in temperature, HCl and water content.

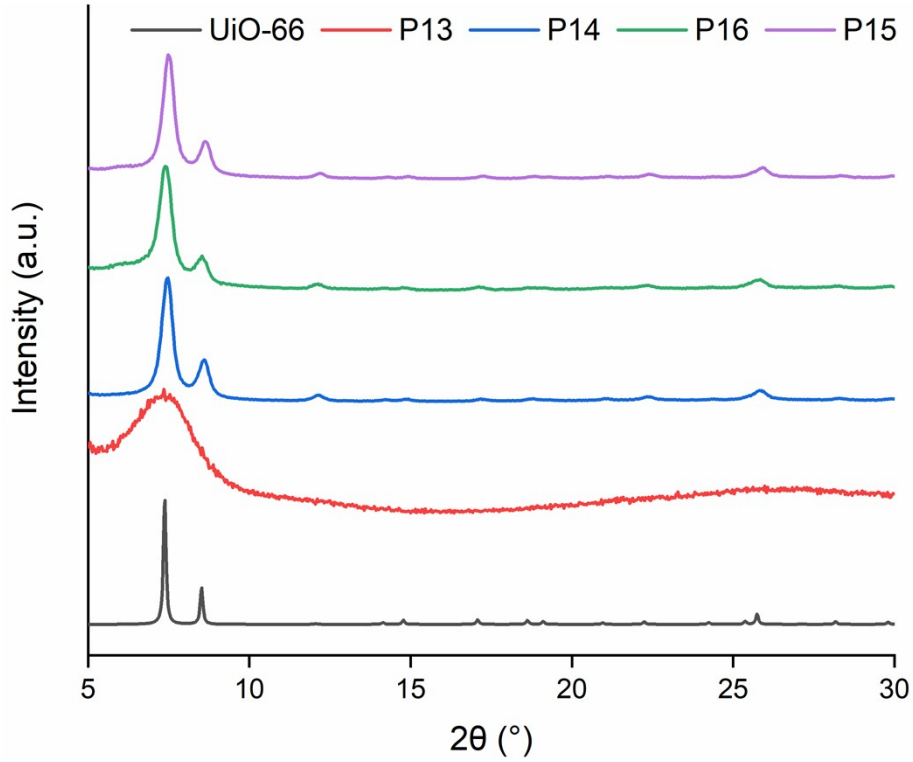

Figure S5: PXRD pattern of samples synthesised starting from H_2BDC in MeOH in the conditions reported in Table S3.

Table S4: syntheses from 1 mmol MMT/DMT, 1 mmol $ZrOCl{\cdot}8H_2O$ in water (10 mL total volume) at 90 °C. Workup protocol: 10 mL 0.1 M TEA in MeOH, 60 min x 2; 10 mL MeOH, 60 min x 2; 10 mL acetone, 60 min x 1.

Sample	Organic precursor	HCl (eq)	H_2O (eq)	Time (h)	Yield (mg)	Phase
P17	MMT	15	15	5	208	**fcu**
P18	DMT	15	15	26	192	**fcu/reo**

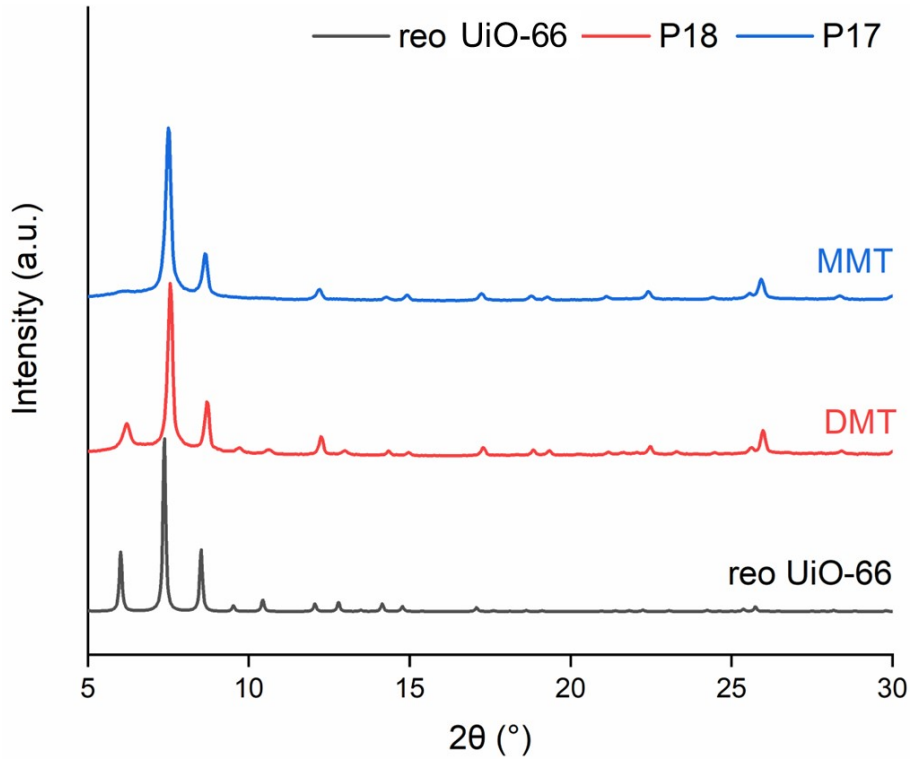

Figure S6: PXRD patterns of P17 (blue) and P18 (red). Reaction conditions: 15 eq AA, 15 eq HCl, 5 h.

Design of experiments

The preliminary screening experiments using DMT were performed starting directly from the commercially available DMT pills, which tend to react slowly due to their morphology. To increase the surface/volume ratio, it was tried to grind DMT, but this approach was not successful because of the sticky nature of the solid, that makes it very difficult to accurately weigh and transfer the DMT powder. It was also tried to solubilise DMT in AA and then add it to the water-based reaction mixture, causing the reprecipitation of diesters in the form of flakes, with a much higher exposed surface than commercially available pills. This strategy was not successful either, because, despite the stirring, these flakes tend to stick to the internal walls of the glass vial, without being able to react completely.

Table S5: syntheses from 1 mmol DMT/BHET, 1 mmol $ZrOCl{\cdot}8H_2O$ in water (10 mL total volume) at 90 °C. Workup protocol: 10 mL 0.1 M TEA in MeOH, 60 min x 2; 10 mL MeOH, 60 min x 2; 10 mL acetone, 60 min x 1.

Sample	Diester	AA (eq)	HCl (eq)	Time (h)	Yield (mg)	Phase	FWHM[a] (°)
P2	DMT	10	10	5	87	**hcp**	0.25
P2_b	BHET	10	10	5	116	**hcp**	-[b]
P6	DMT	20	20	5	100	**fcu/reo**	0.16
P6_b	BHET	20	20	2	72	**fcu**	0.17

[a] FWHM of reflection 111 for **fcu** phase and reflection 101 for **hcp** phase (both reflections are located at 7.3°);
[b] the 101 reflection is superimposed with the 100 reflection.

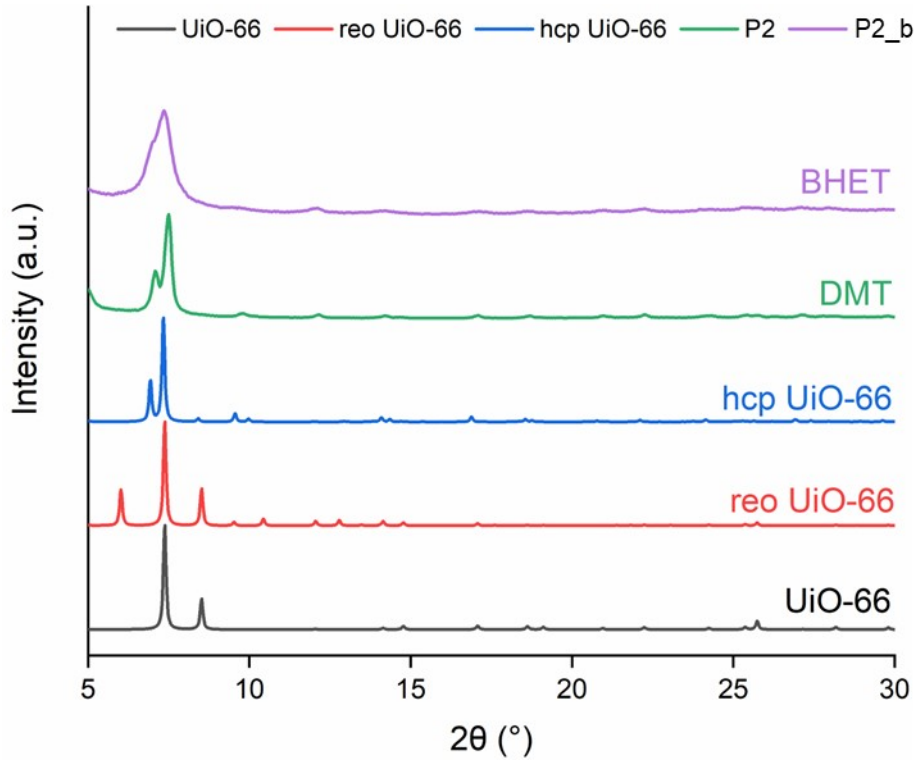

Figure S7: PXRD pattern of P2 (green) and P45 (purple). Reaction conditions: 10 eq AA, 10 eq HCl, 24 h.

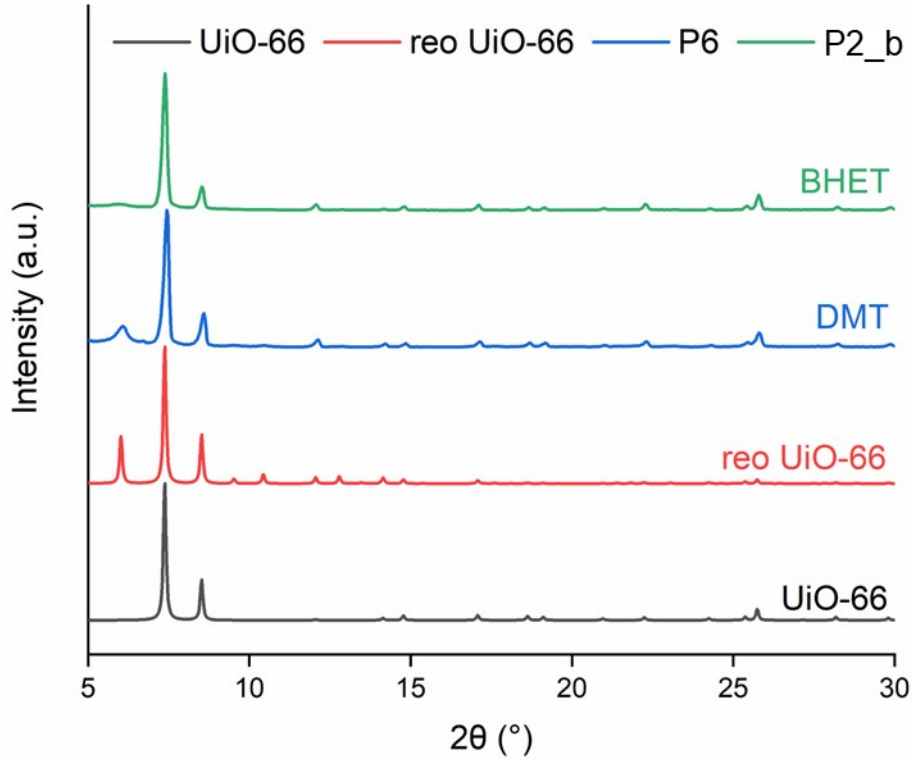

Figure S8: PXRD pattern of P6 (blue) and P46 (green). Reaction conditions: 20 eq AA, 20 eq HCl, 24 h.

CCD allows to estimate a quadratic model with linear, quadratic and interaction terms. In this way is possible to estimate the maximum and minimum of the calculated function, like the yield in a synthesis process. Mathematically, this type of model can be written as reported in **Equation S1**.

$$Y = b_0 + \sum_{i=1}^{k} b_i x_i + \sum_{i=1}^{k} b_{ii} x^2{}_i + \sum_{i<j} \sum b_{ij} x_i x_j$$

Equation S1

Where:

- ***Y*** (dependent variable) is the response
- b_0 is the intercept, and it is a constant. It sets average value of the function
- b_j is correlated to the effect of the variable ***i***
- b_{ii} is correlated to the combined effect of variable ***i*** with itself, and it is used to determine the curvature of the function
- b_{ij} is correlated to the combined effect of variables ***i*** and ***j***, and it expresses the synergic effect of these variables
- x_i and x_j are the variables considered

Table S6: regression coefficients of experimental design and their statistical significance

β_0	41
β_1	-8.5**
β_2	-2.6*
β_3	-1.0
β_{12}	-1.0
β_{13}	2.5*
β_{23}	-0.75
β_{11}	-9.28**
β_{22}	-8.78**
β_{33}	2.22
R^2	0.972

** 95% ≤ Significance < 99%; * 90% ≤ Significance < 95%

The analysis of regression coefficients in Table S6 shows that RME has a significant dependence on the linear term associated with AA (β_1), which negatively influences the

response, and the quadratic terms associated with AA (β_{11}) and HCl (β_{22}), both of whom have a negative effect on the response. Instead, the regression coefficient associated with reaction time (β_3) seems not to be very significant, indicating that time is not a very influential parameter on RME within the investigated range. Furthermore, synergic effects seem to be very limited, except for the coefficient associated to the synergic effect of AA and time (β_{13}).

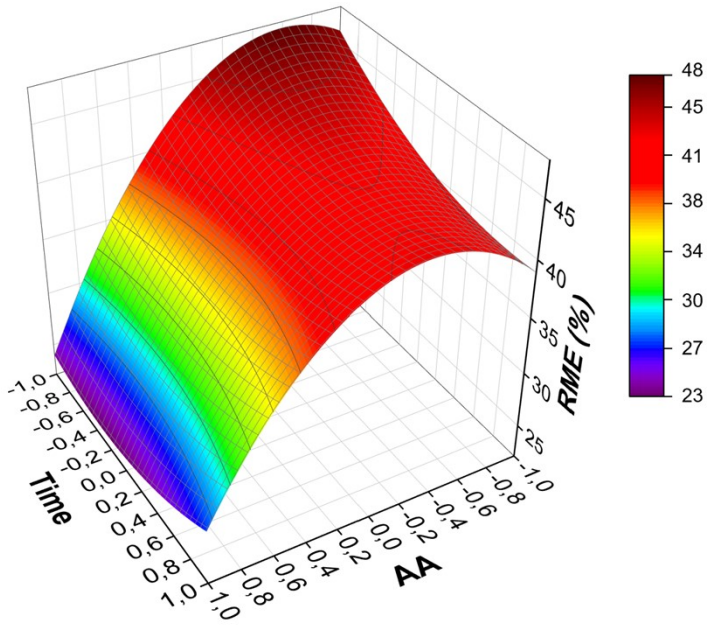

Dimensionless variable	-1	0	1
AA (eq)	5	15	25
Time (h)	5	16	26

HCl = 0 (15 eq)

Figure S9. Response surface for RME (%) as a function of AA and time at fixed HCl amount of 15 eq.

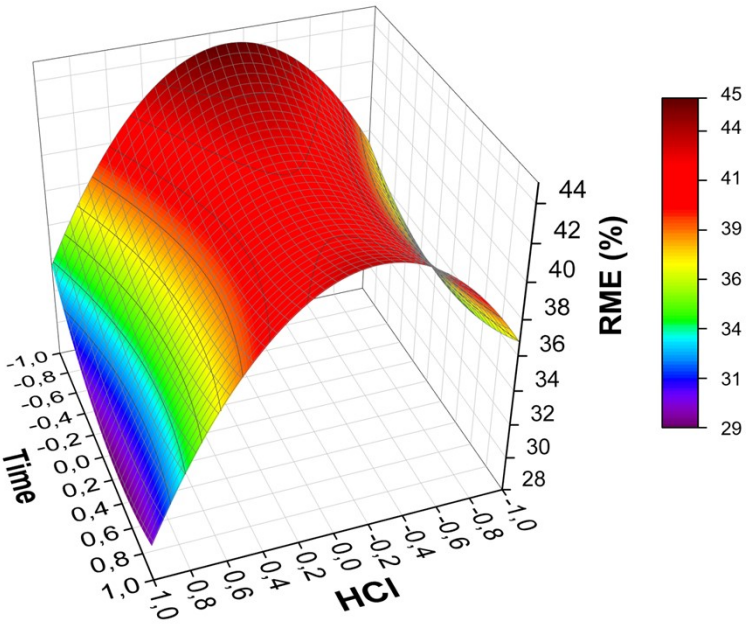

Dimensionless variable	-1	0	1
HCl (eq)	5	15	25
Time (h)	5	16	26

AA = 0 (15 eq)

Figure S10. Response surface for RME (%) as a function of HCl and time at fixed AA amount of 15 eq.

Table S7: univariate analysis of the effect of the amount of AA on RME and phase selection.

Sample	AA (eq)	HCl (eq)	Time (h)	RME (%)	Phase	FWHM[a] (°)
P26	5	5	26	34	**hcp**	- [b]
P20	25	5	26	21	**hcp** + **fcu** + H_2BDC	- [c]
P25	5	25	26	25	**fcu** + H_2BDC	- [c]
P22	25	25	26	16	H_2BDC + **fcu**	- [c]
P27	5	15	16	42	**hcp**	- [b]
P33	15	15	16	42	**fcu**	0.19
P32	25	15	16	21	**fcu** + H_2BDC	- [c]
P24	5	5	5	36	**hcp**	- [b]
P21	25	5	5	21	**fcu**	0.43
P19	5	25	5	38	**fcu**	0.49
P23	25	25	5	11	H_2BDC	- [c]

[a] FWHM of reflection 111 for **fcu** phase and reflection 101 for **hcp** phase (both reflections are located at 7.3°); [b] the 101 reflection is superimposed with the 100 reflection; [c] FWHM not reported for mixed phase systems and when H_2BDC is the only crystalline phase.

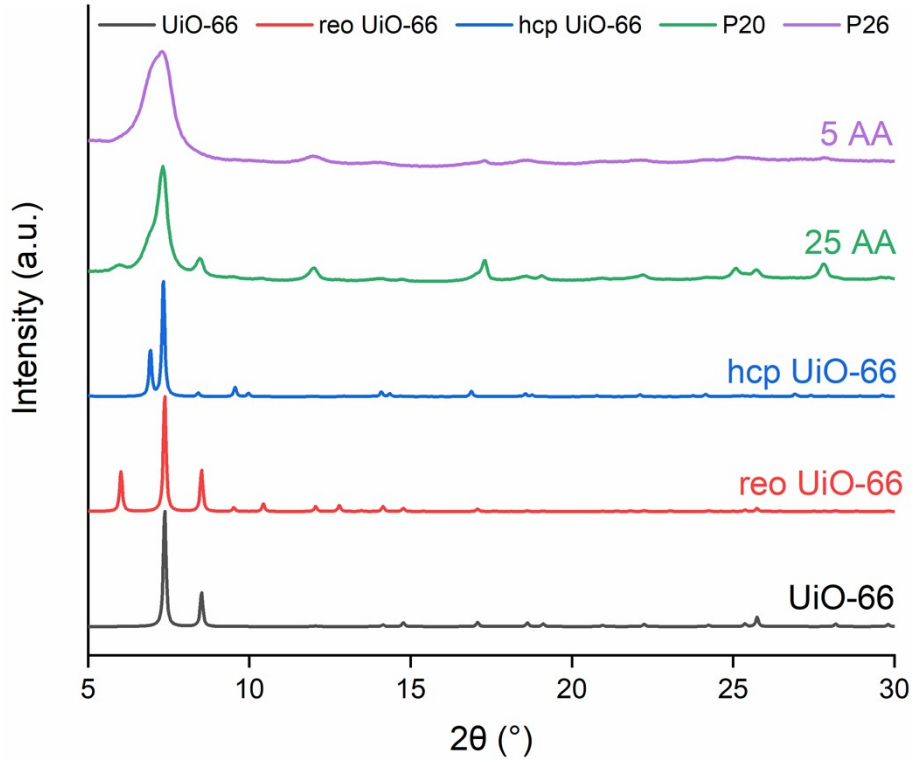

Figure S11: PXRD patterns of P20 (blue) and P26 (purple). Reaction conditions: 5 eq HCl, 26 h.

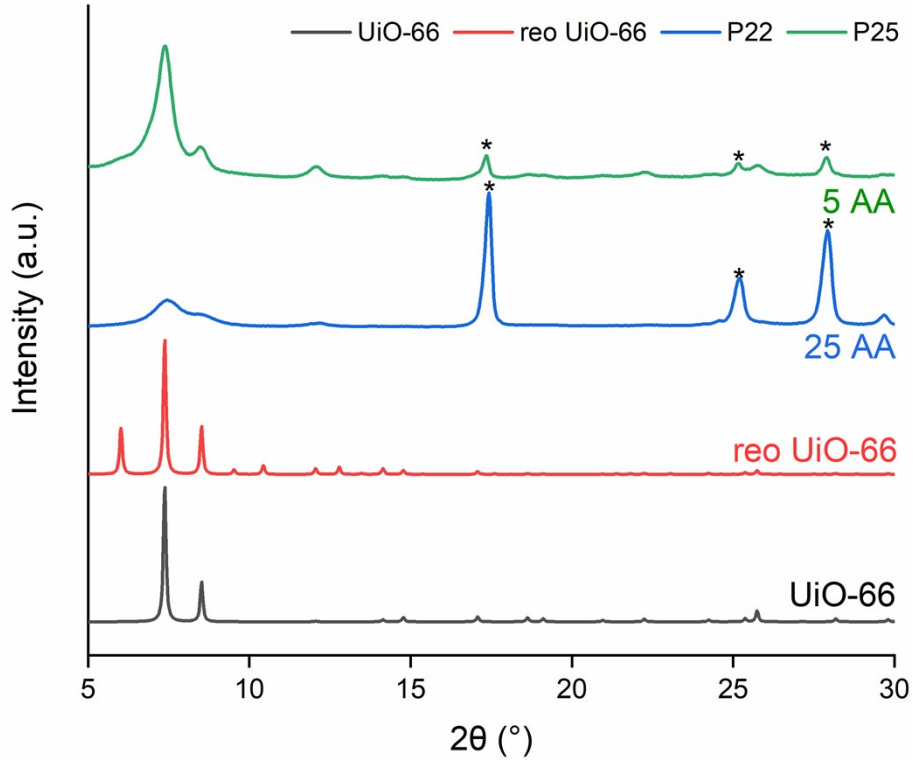

Figure S12: PXRD patterns of P22 (blue) and P25 (green). Reaction conditions: 25 eq HCl, 26 h. * indicates peaks associated with crystallised H_2BDC.

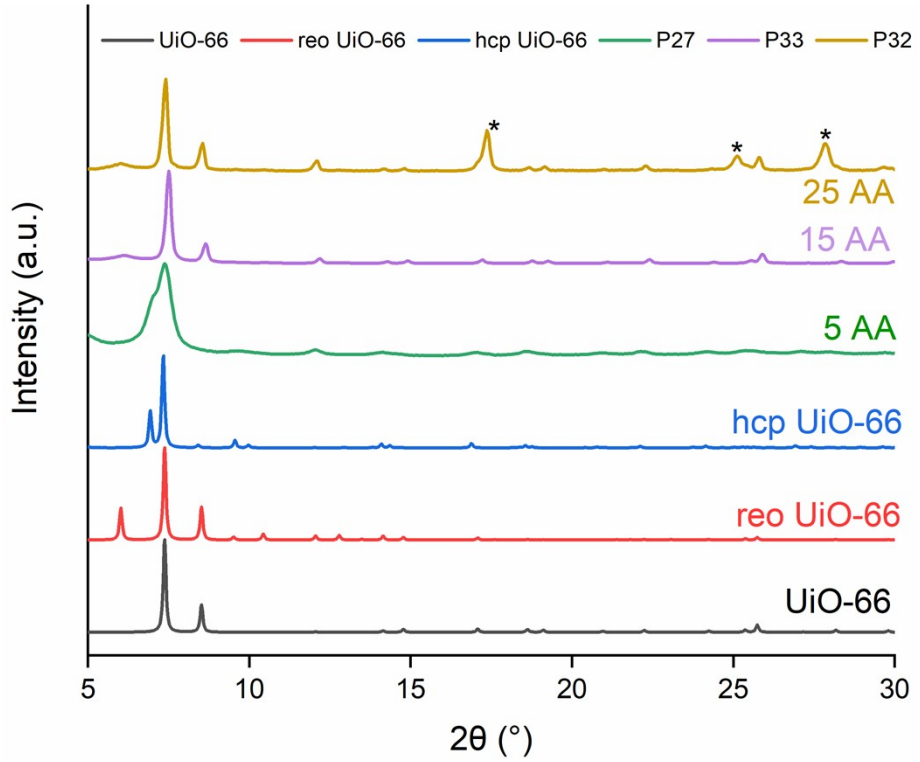

Figure S13: PXRD pattern of P27 (green), P33 (purple) and P32 (yellow). Reaction conditions: 15 eq HCl, 16 h. * indicates peaks associated with crystallized H_2BDC

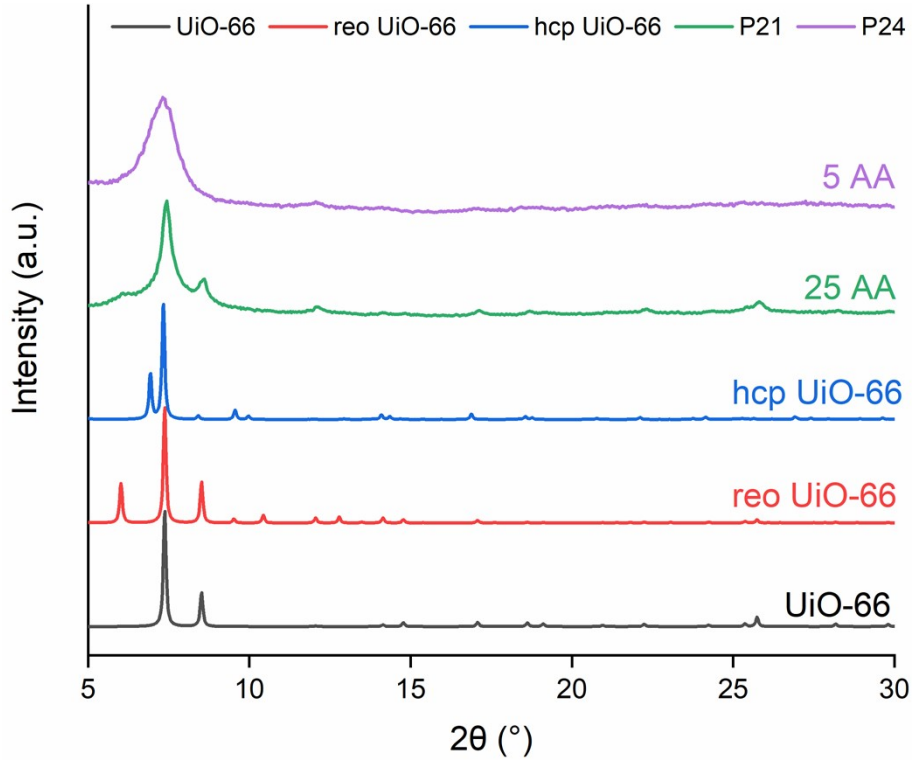

Figure S14: PXRD pattern of P21 (green), P24 (purple). Reaction conditions: 5 eq HCl, 5 h.

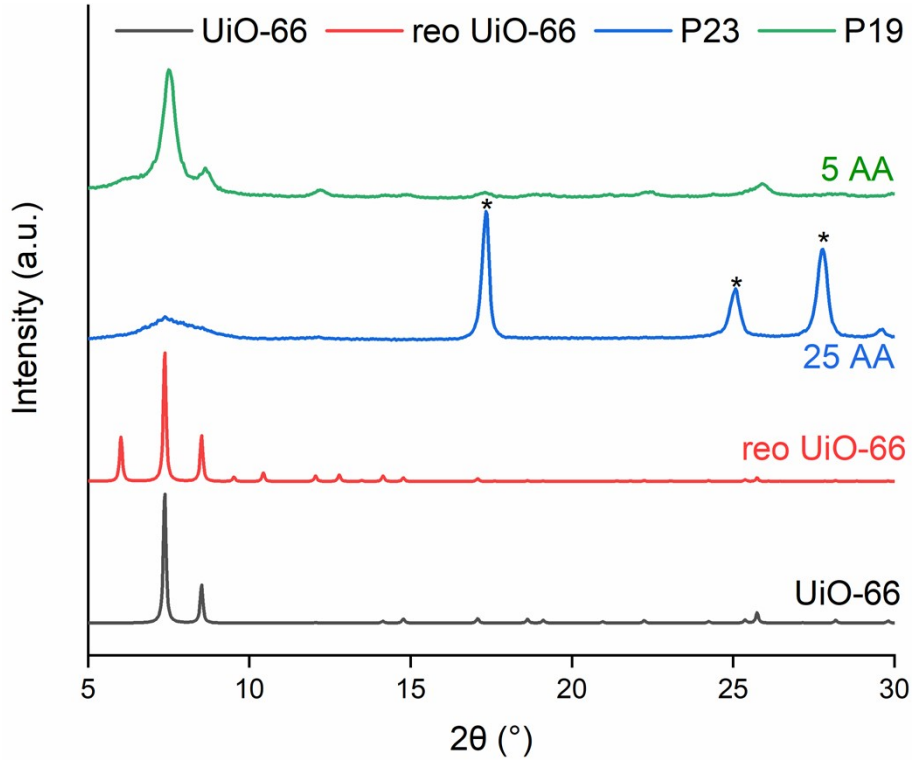

Figure S15: PXRD pattern of P23 (blue), P19 (green). Reaction conditions: 25 HCl, 5 h, * indicates peaks associated with crystallised H_2BDC.

Table S8: univariate analysis of the effect of the amount of HCl on RME and phase selection.

Sample	AA (eq)	HCl (eq)	Time (h)	RME (%)	Phase	FWHM[a] (°)
P21	25	5	5	21	**fcu**	0.43
P23	25	25	5	11	H_2BDC	- [c]
P24	5	5	5	36	**hcp**	- [b]
P19	5	25	5	38	**fcu**	0.49
P28	15	5	16	34	**fcu**	0.46
P33	15	15	16	42	**fcu**	0.19
P30	15	25	16	30	**fcu**	0.17
P20	25	5	26	21	**hcp** + **fcu** + H_2BDC	- [c]
P22	25	25	26	16	H_2BDC	- [c]
P26	5	5	26	34	**hcp**	- [b]
P25	5	25	26	25	**fcu**	0.59

[a] FWHM of reflection 111 for **fcu** phase and reflection 101 for **hcp** phase (both reflections are located at 7.3°); [b] the 101 reflection is superimposed with the 100 reflection; [c] FWHM not reported for mixed phase systems and when H_2BDC is the only crystalline phase.

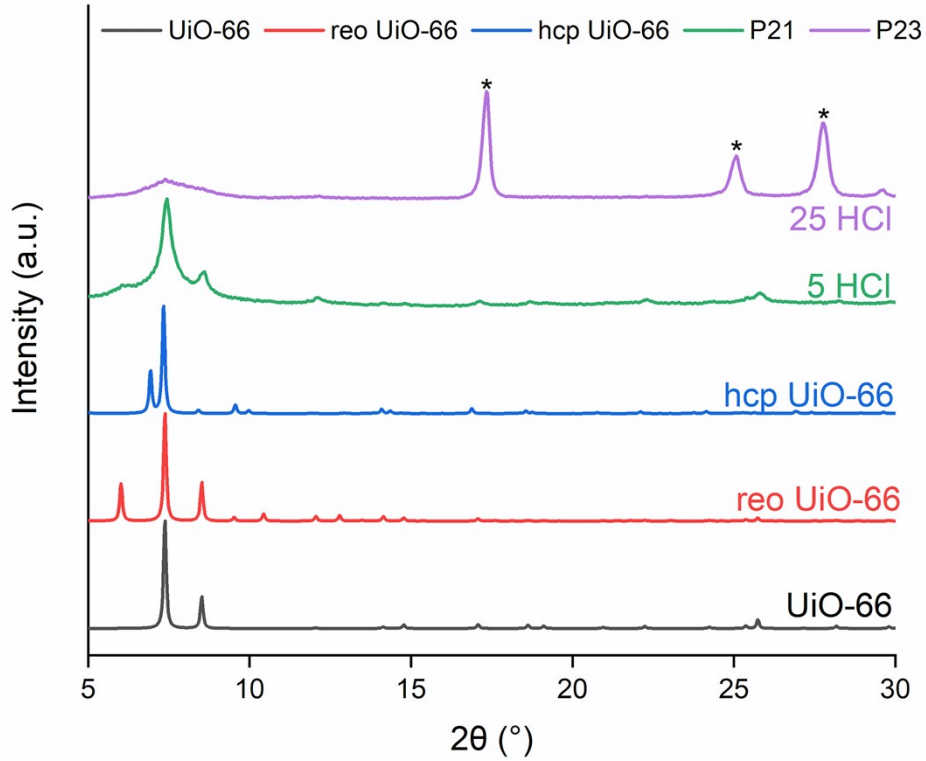

Figure S16: PXRD pattern of P21 (green) and P23 (purple). Reaction conditions: 25 AA, 5 h. * indicates peaks associated with crystallised H_2BDC

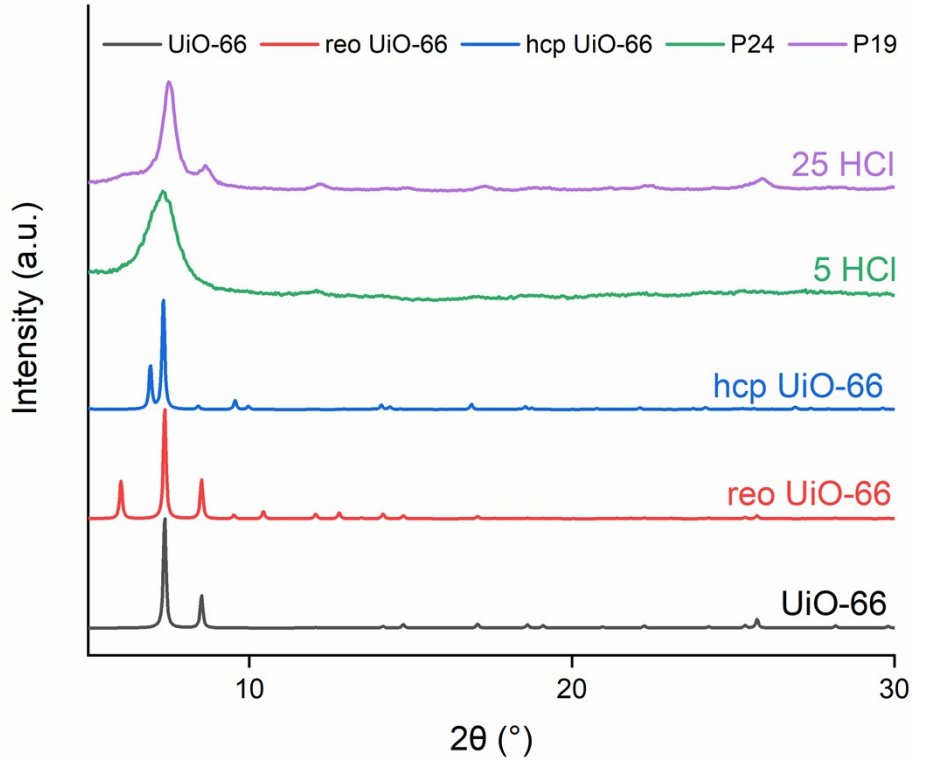

Figure S17: PXRD patterns of P24 (green) and P19 (purple). Reaction conditions: 5 AA, 5 h.

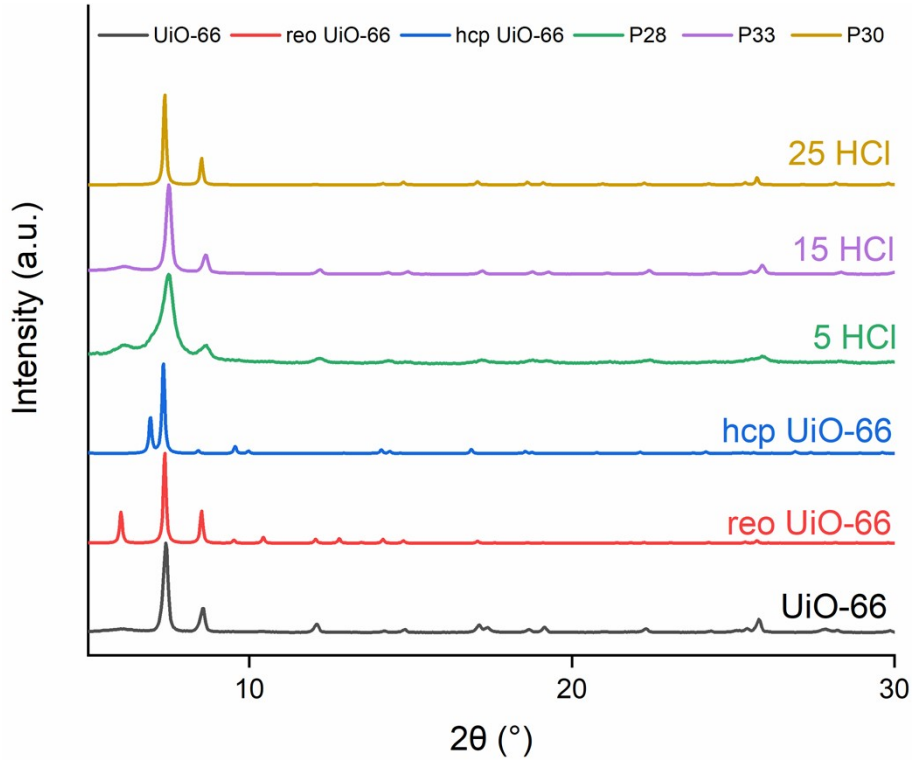

Figure S18: PXRD pattern of P28 (green) and P33 (purple) and P30 (yellow). Reaction conditions: 15 AA, 16 h.

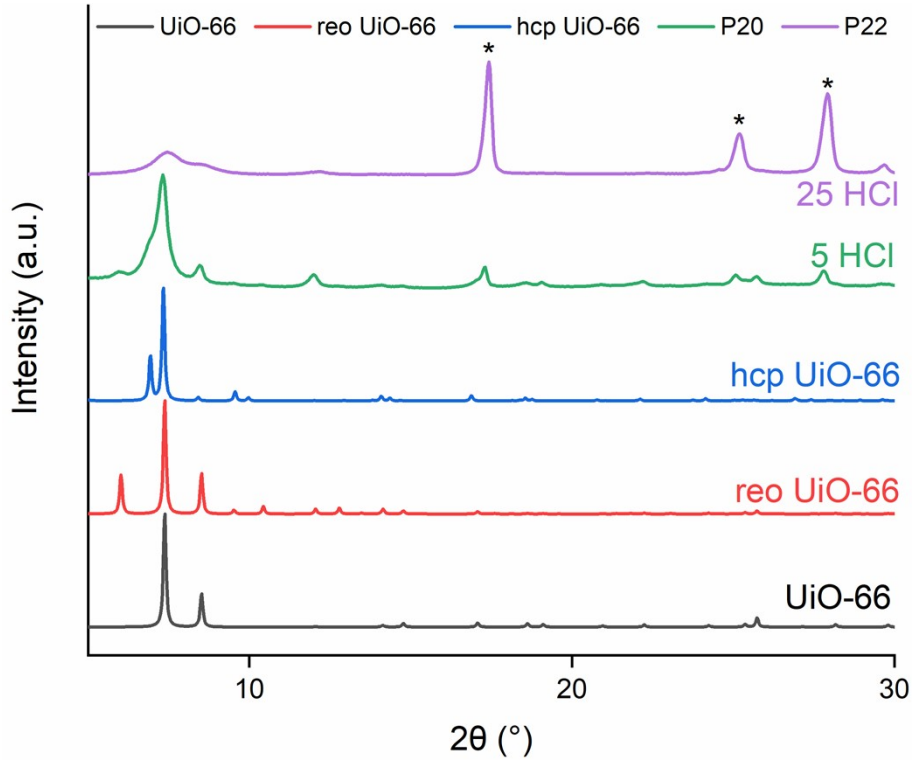

Figure S19: PXRD pattern of P20 (green) and P22 (purple). Reaction conditions: 25 AA, 26 h. * indicates peaks associated with crystallised H_2BDC.

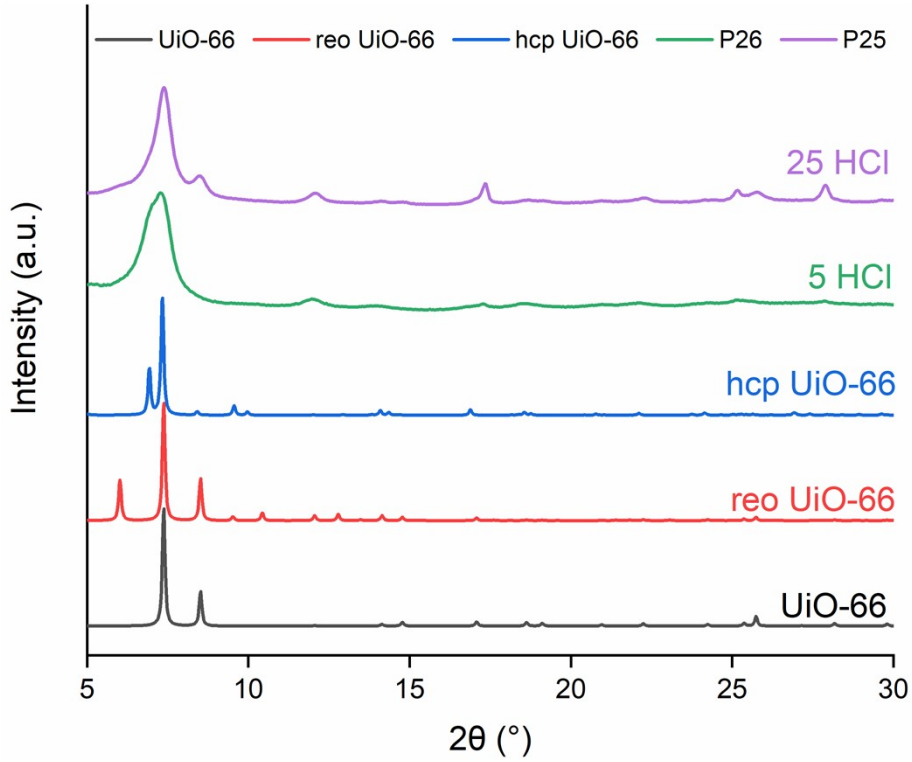

Figure S20: PXRD pattern of P26 (green) and P25 (purple). Reaction conditions: 5 AA, 26 h.

Table S9: univariate analysis of the effect of reaction time on RME and phase selection.

Sample	AA (eq)	HCl (eq)	Time (h)	RME (%)	Phase	FWHM[a] (°)
P19	5	25	5	38	**fcu**	0.49
P25	5	25	26	25	**fcu** + H_2BDC	- [c]
P21	25	5	5	21	**fcu**	0.43
P20	25	5	26	21	**fcu** + **hcp** + H_2BDC	- [c]
P29	15	15	5	43	**fcu**	0.17
P33	15	15	16	42	**fcu**	0.19
P31	15	15	26	43	**fcu**	0.22
P23	25	25	5	11	H_2BDC	- [c]
P22	25	25	26	16	H_2BDC + **fcu**	- [c]
P24	5	5	5	36	**hcp**	- [b]
P26	5	5	26	34	**hcp**	- [b]

[a] FWHM of reflection 111 for **fcu** phase and reflection 101 for **hcp** phase (both reflections are located at 7.3°); [b] the 101 reflection is superimposed with the 100 reflection; [c] FWHM not reported for mixed phase systems and when H_2BDC is the only crystalline phase.

Table S10: tests performed to optimise the reaction time. Workup protocol: 10 mL DMF, 90 min x 2; 10 mL MeOH, 90 min x 2; 10 mL acetone, 90 min x 1.

Sample	AA (eq)	HCl (eq)	Time (h)	RME (%)
P34	15	15	1	10
P35	15	15	2	34
P36	15	15	3	34
P37	15	15	4	35
P38	15	15	5	34

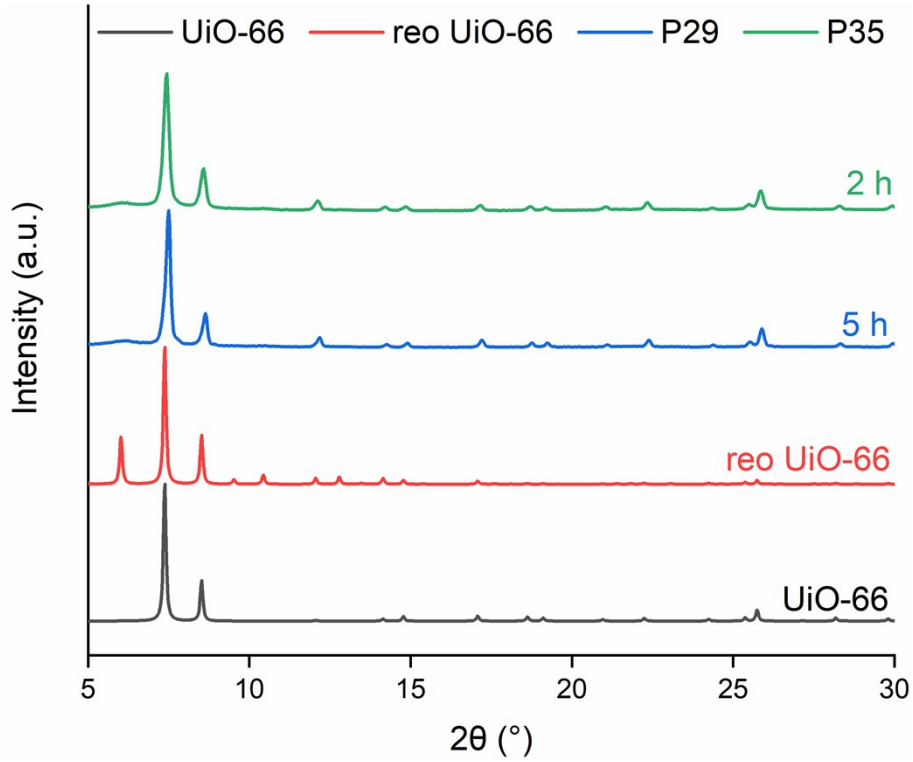

Figure S21: PXRD patterns of P29 (blue) and P35 (green). Reaction conditions: 15 AA and 15 HCl.

Optimisation of the workup protocol

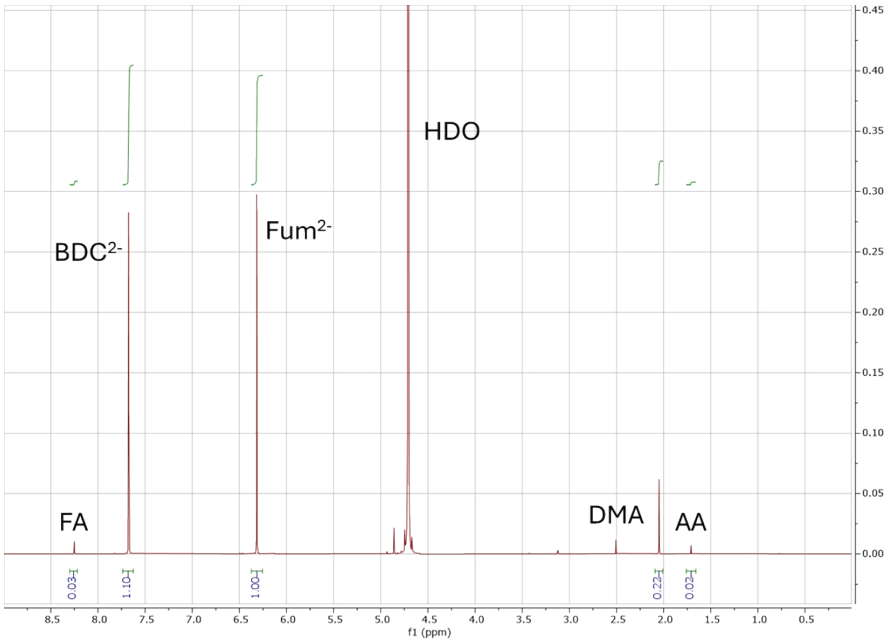

Figure S22: Quantitative ^{1}H-NMR spectrum of P38 (18.0 mg) digested in 1.0 mL of 1.0 M NaOH in D_2O with 0.10 M fumaric acid as internal standard. The signal of BDC^{2-} at 7.6 ppm accounts for four aromatic protons, therefore its integral must be divided by four to obtain the values comparable with that of fumarate (Fum^{2-}, 1.00) at 6.3 ppm, which accounts for only two protons. The signals of dimethylamine (DMA) at 2.1 ppm (six protons) and formic acid (FA) at 8.3 ppm (one proton), derived from hydrolysis of residual DMF in the pores, are not significant. The signal of AA (three protons) at 1.7 ppm is also not significant, indicating that AA is not retained as a defect-compensating species in the MOF. Given the concentration of Fum^{2-} is 0.10 M, the concentration of BDC^{2-} is found to be 0.055 M, corresponding to 9.0 mg (50 wt%). The chemical formula of P38 can be derived by assuming the general formula $Zr_6O_4(OH)_4(BDC)_{6-x}(OH/H_2O)_{2x}$, where the value of x can be derived by imposing that the wt% of BDC^{2-} be 50%, leading to $Zr_6O_4(OH)_4(BDC)_{4.68}(OH/H_2O)_{2.64}$.

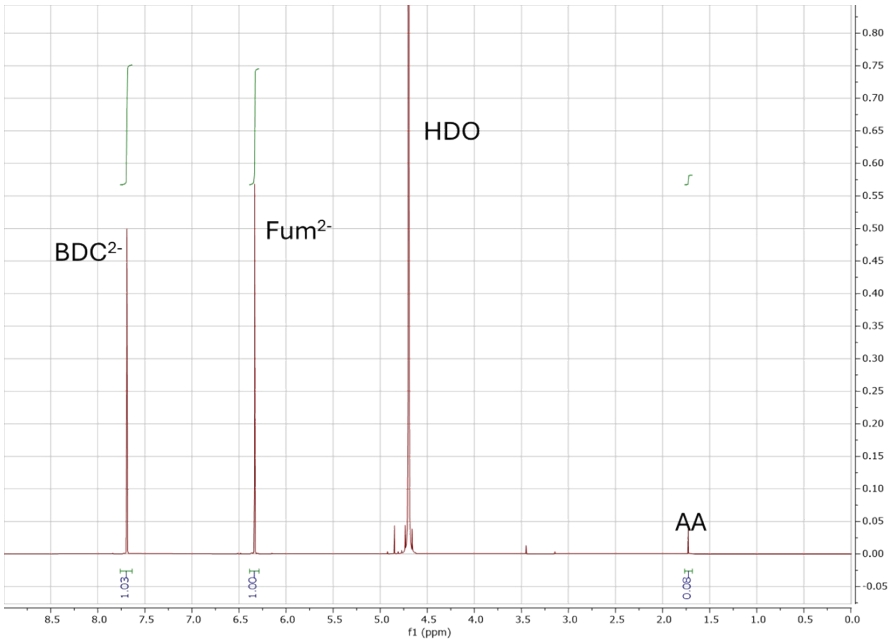

Figure S23: Quantitative ^{1}H-NMR spectrum of P29 (14.2 mg) digested in 1.0 mL of 1.0 M NaOH in D_2O with 0.10 M fumaric acid as internal standard. The signals of BDC^{2-} at 7.6 ppm account for four aromatic protons, therefore its integral must be divided by four to obtain the values comparable with that of fumarate (Fum^{2-}) at 6.3 ppm, which accounts for only two protons. The signal of AA (three protons) at 1.7 ppm is not significant, indicating that AA is not retained as a defect-compensating species in the MOF. Given the concentration of Fum^{2-} is 0.10 M, the concentration of BDC^{2-} is found to be 0.052 M, corresponding to 8.5 mg (60 wt%). The higher wt% of BDC^{2-} than what found for P38 suggests that excess of linker is present in the pores of P29, as the two samples only differ for the workup procedure. The chemical formula of P29 can be derived by assuming the same formula of P38 and accounting for the presence of excess H_2BDC as follows: $Zr_6O_4(OH)_4(BDC)_{4.68}(OH/H_2O)_{2.64}\square_y(H_2BDC)$. The value of y is found to be 2.36.

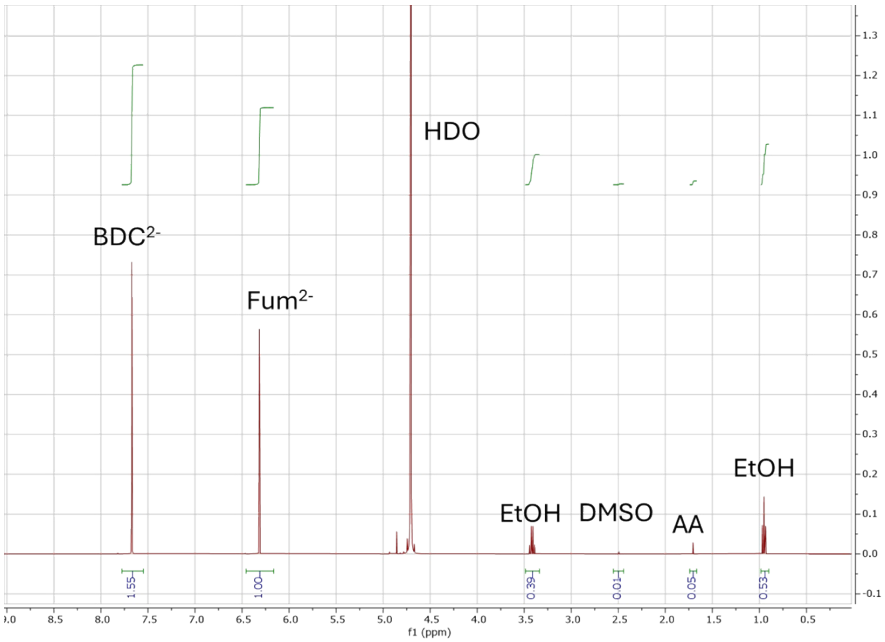

Figure S24: Quantitative ^{1}H-NMR spectrum of P39 (27.6 mg) digested in 1 mL of 1 M NaOH in D_2O with 0.10 M fumaric acid as internal standard. The signals of BDC^{2-} at 7.6 ppm account for four aromatic protons, therefore its integral must be divided by four to obtain the values comparable with that of fumarate (Fum^{2-}, 1.00) at 6.3 ppm, which accounts for only two protons. The signal of DMSO (six protons) at 2.5 ppm is not significant, proving that the washing procedure with water is effective at removing DMSO from the pores. The signal of AA (three protons) at 1.7 ppm is also not significant, indicating that AA is not retained as a defect-compensating species in the MOF. The signals of EtOH at 1.0 ppm (three protons) and 3.4 ppm (two protons) indicate that some of the solvent used for the last step of the workup is still present in the pores. Given the concentration of Fum^{2-} is 0.10 M, the concentration of BDC^{2-} is found to be 0.078 M, corresponding to 12.8 mg (46 wt%), whereas the concentration of EtOH is 0.035 M, corresponding to 1.6 mg (6 wt%). The lower wt% of BDC^{2-} than what found for P38 is likely due to the presence of residual solvent in the pores of P39. The chemical formula of P39 can be derived by assuming that all EtOH is physisorbed in the pores and that accounting for a EtOH/BDC^{2-} integral ratio of 0.45, leading to the general formula $Zr_6O_4(OH)_4(BDC)_{6-x}(OH/H_2O)_{2x}\cdot 0.45(6-x)EtOH$. The value of *x* can be derived by imposing that the wt% of BDC^{2-} be 50%, leading to $Zr_6O_4(OH)_4(BDC)_{4.55}(OH/H_2O)_{2.90}\cdot 2.1EtOH$ is derived, which suggests a slightly higher amount of defects than P38.

Characterisation

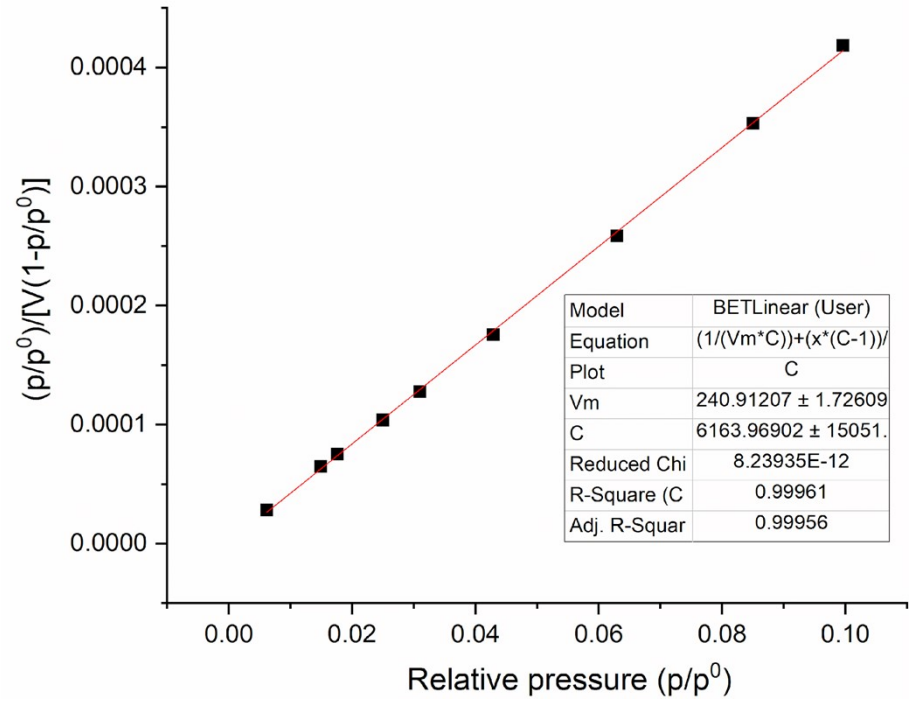

Figure S25: Linear fitting of the BET equation in the relative pressure range 0.008-0.10 for No Defective_UiO-66.

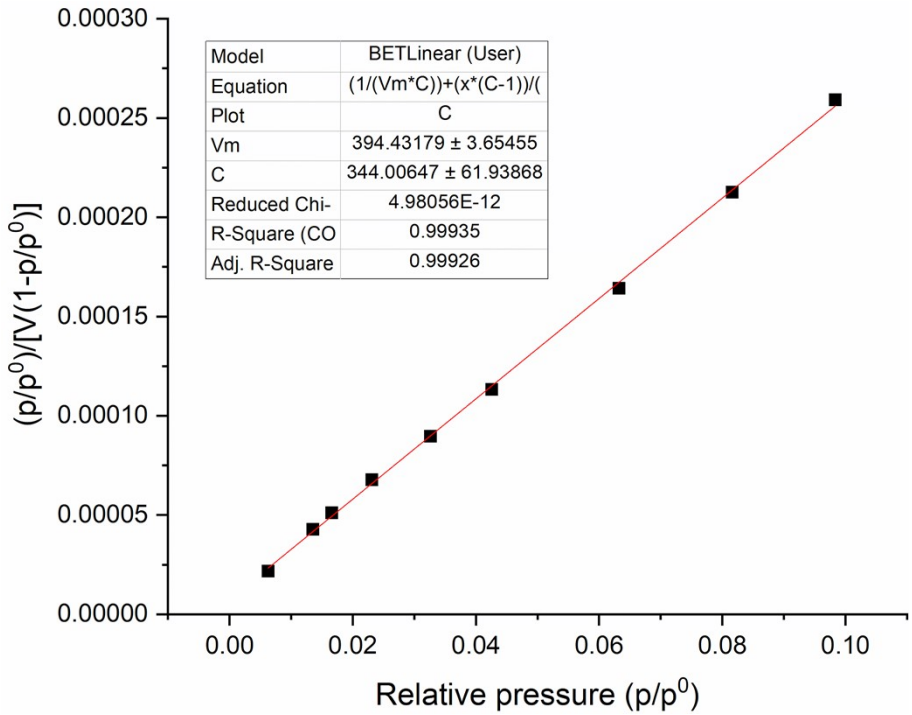

Figure S26: Linear fitting of the BET equation in the relative pressure range 0.008-0.10 for Defective_UiO-66.

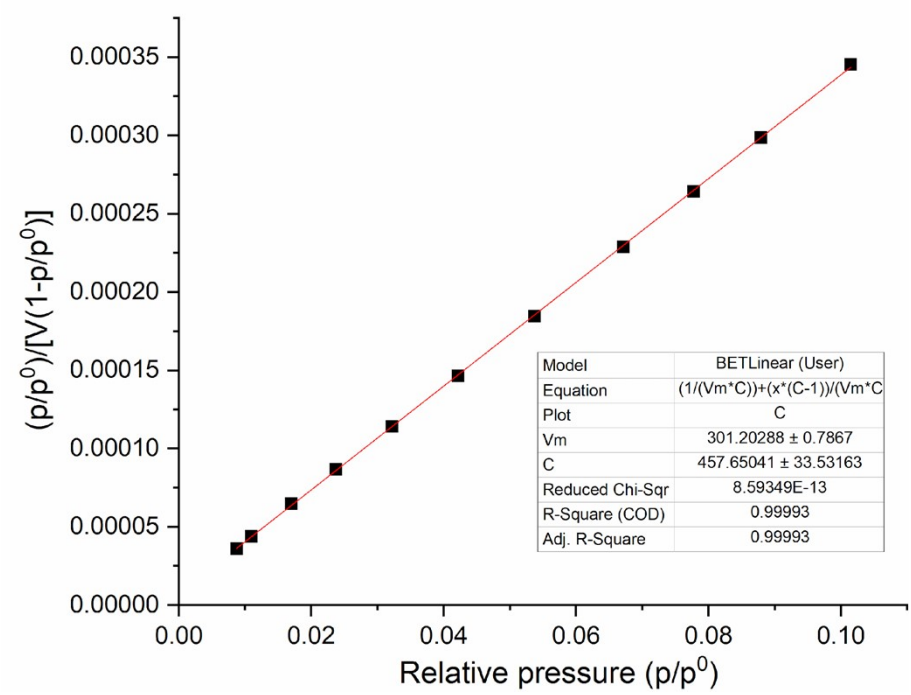

Figure S27: Linear fitting of the BET equation in the relative pressure range 0.008-0.10 for P38.

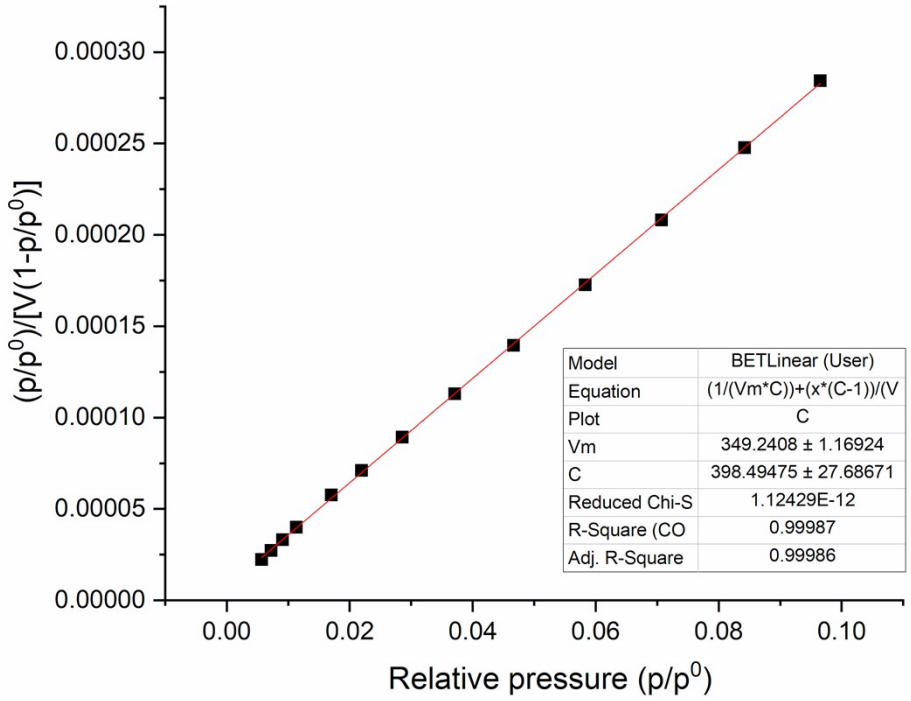

Figure S28: Linear fitting of the BET equation in the relative pressure range 0.008-0.10 for P39.

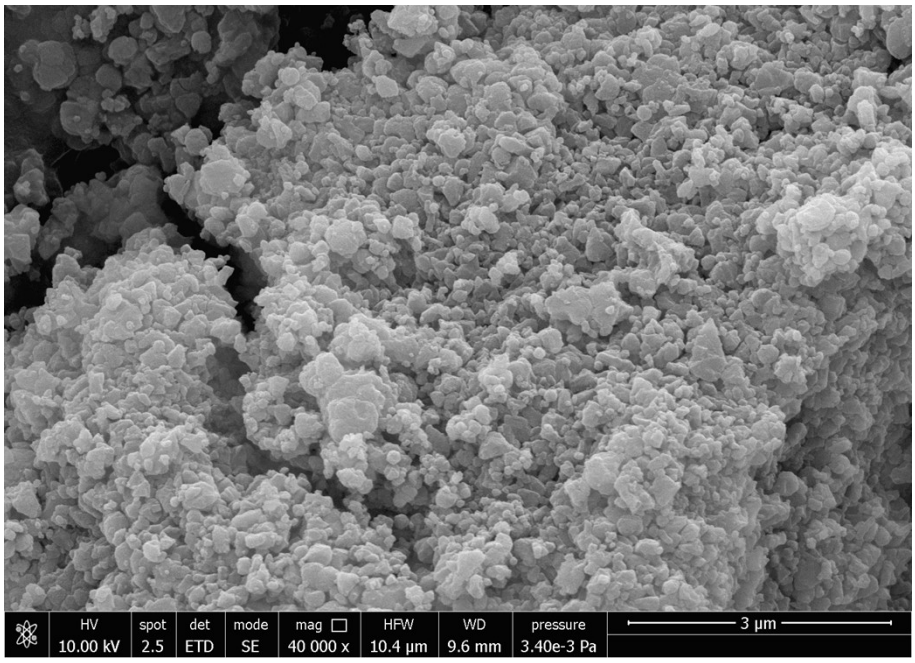

Figure S29: SEM micrograph of P39.

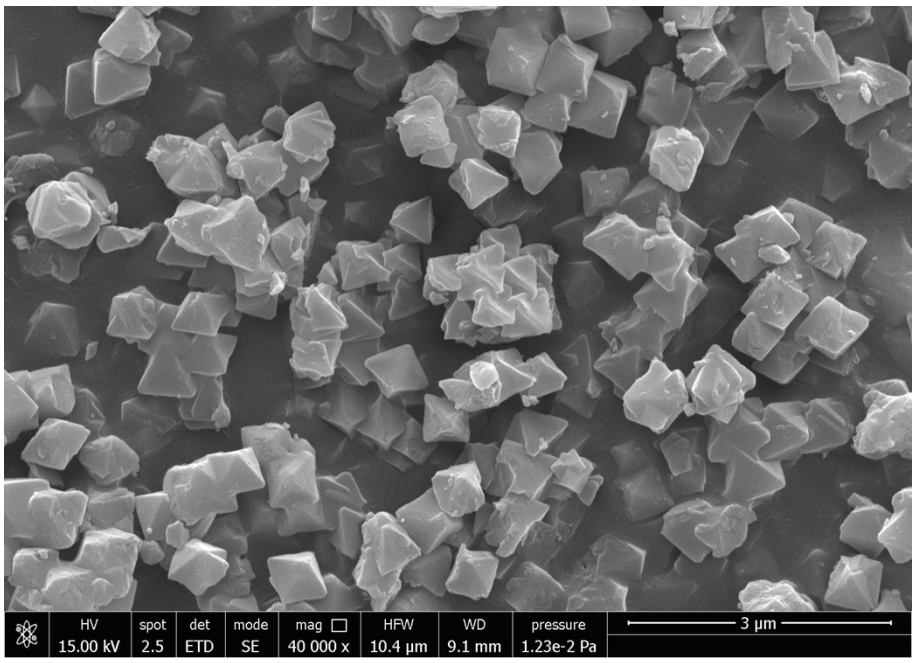

Figure S30: SEM micrograph of Defective_UiO-66.

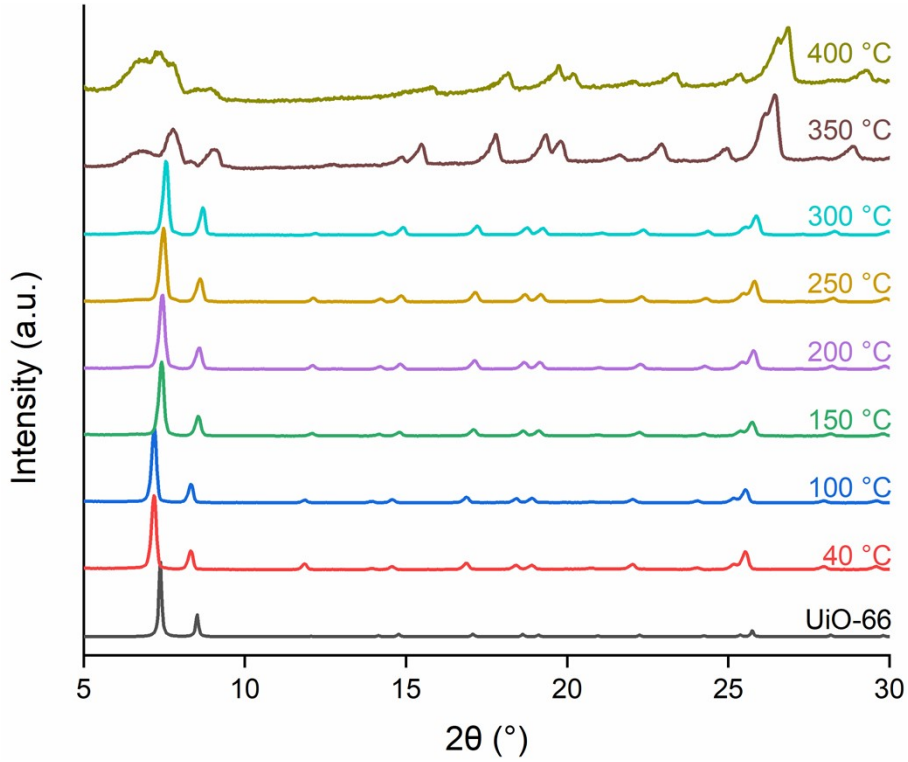

Figure S31: VTPXRD patterns of Defective_UiO-66 from 40 to 400 °C

Synthesis scale up

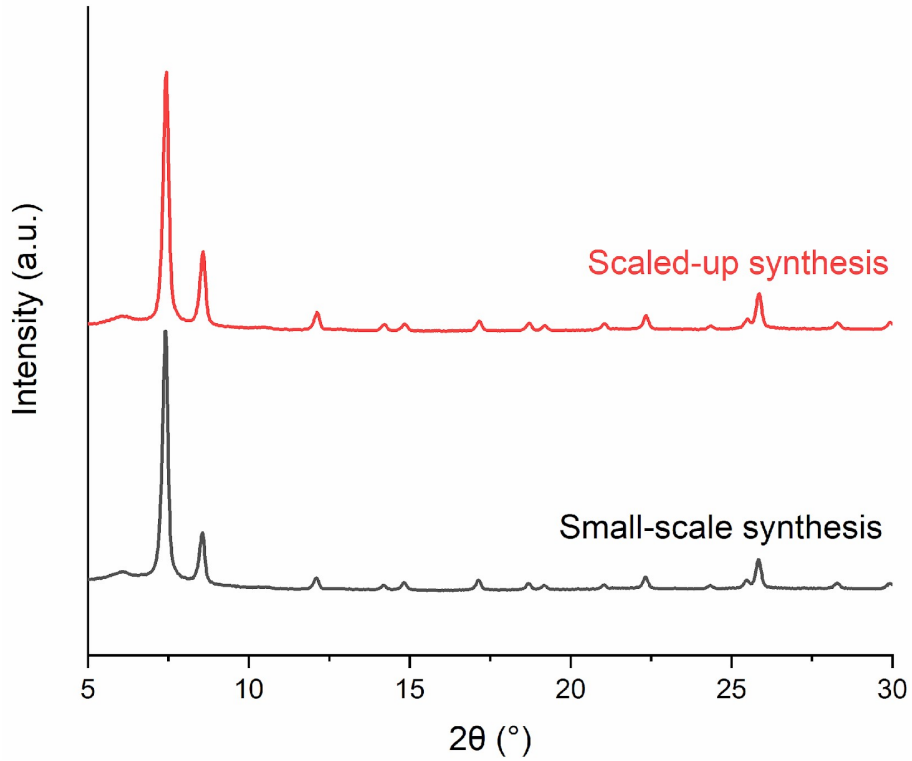

Figure S32: Comparison of the PXRD patterns of P39 (black) and P39_LS (red).

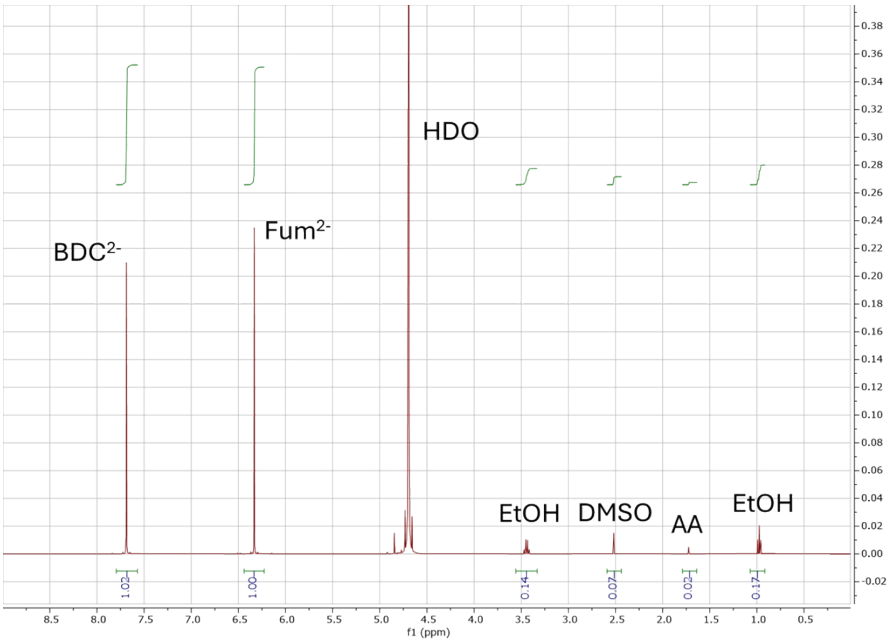

Figure S33: Quantitative ^{1}H-NMR spectrum of P39_LS (16.7 mg) digested in 1.0 mL of 1.0 M NaOH in D_2O with 0.10 M fumaric acid as internal standard. The signals of BDC^{2-} at 7.6 ppm account for four aromatic protons, therefore its integral must be divided by four to obtain the values comparable with that of fumarate (Fum^{2-}, 1.00) at 6.3 ppm, which accounts for

only two protons. The signal of DMSO at 2.5 ppm (six protons) is not significant, proving that the washing procedure with water is effective at removing DMSO from the pores. The signal of AA at 1.7 ppm (three protons) is also not significant, indicating that AA is not retained as a defect-compensating species in the MOF. The signals of EtOH at 1.0 ppm (three protons) and 3.4 ppm (two protons) indicate that some of the solvent used for the last step of the workup is still present in the pores. Given the concentration of Fum^{2-} is 0.10 M, the concentration of BDC^{2-} is found to be 0.051 M, corresponding to 8.4 mg (50 wt%), whereas the concentration of EtOH is 0.009 M, corresponding to 0.4 mg (2 wt%). The chemical formula of P39 can be derived by assuming that all EtOH is physisorbed in the pores and that accounting for a EtOH/BDC^{2-} integral ratio of 0.18, leading to the general formula $Zr_6O_4(OH)_4(BDC)_{6-x}(OH/H_2O)_{2x}\cdot 0.18(6-x)EtOH$. The value of x can be derived by imposing that the wt% of BDC^{2-} be 50%, leading to $Zr_6O_4(OH)_4(BDC)_{4.90}(OH/H_2O)_{2.20}\cdot 0.9EtOH$ is derived, which suggests a slightly lower amount of defects than P39.

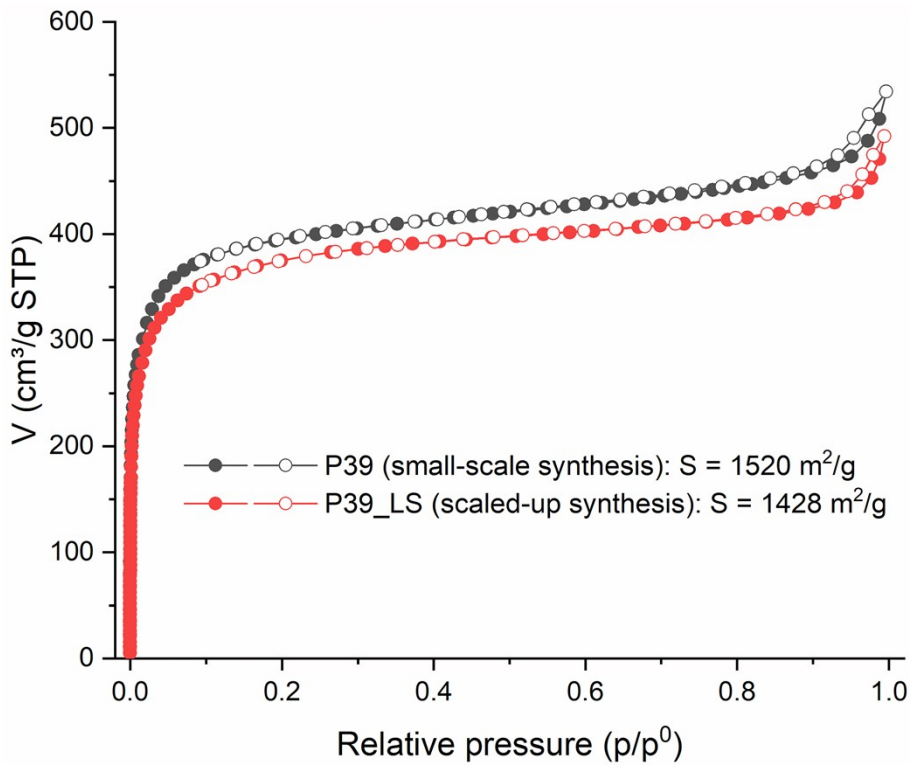

Figure S34: Comparison of the N_2 adsorption/desorption isotherms at 77 K of P39 (black) and P39_LS (red).

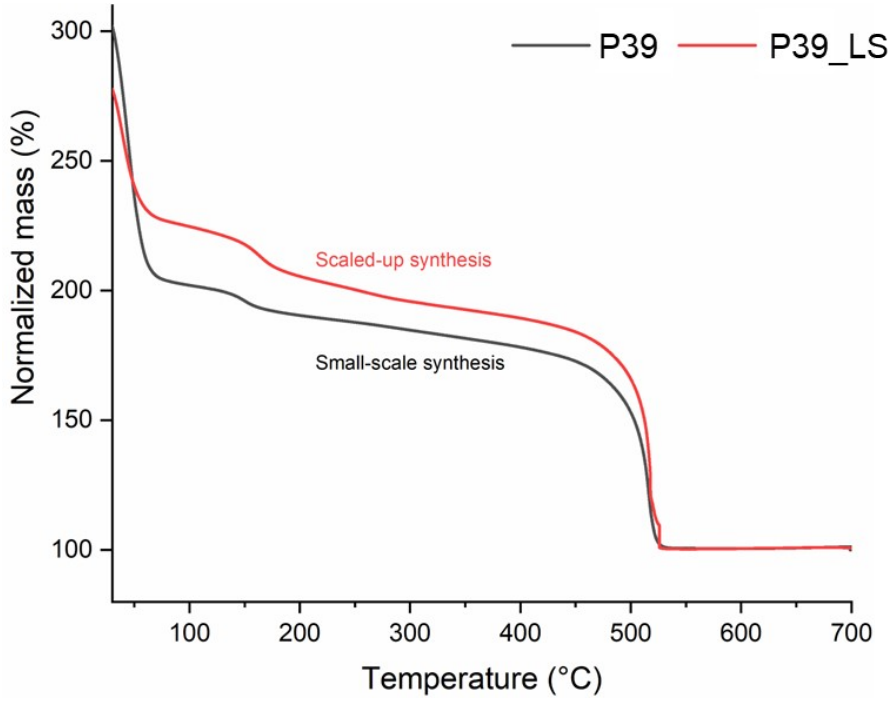

Figure S35: Comparison of the TG curves of P39 (black) and P39_LS (red).

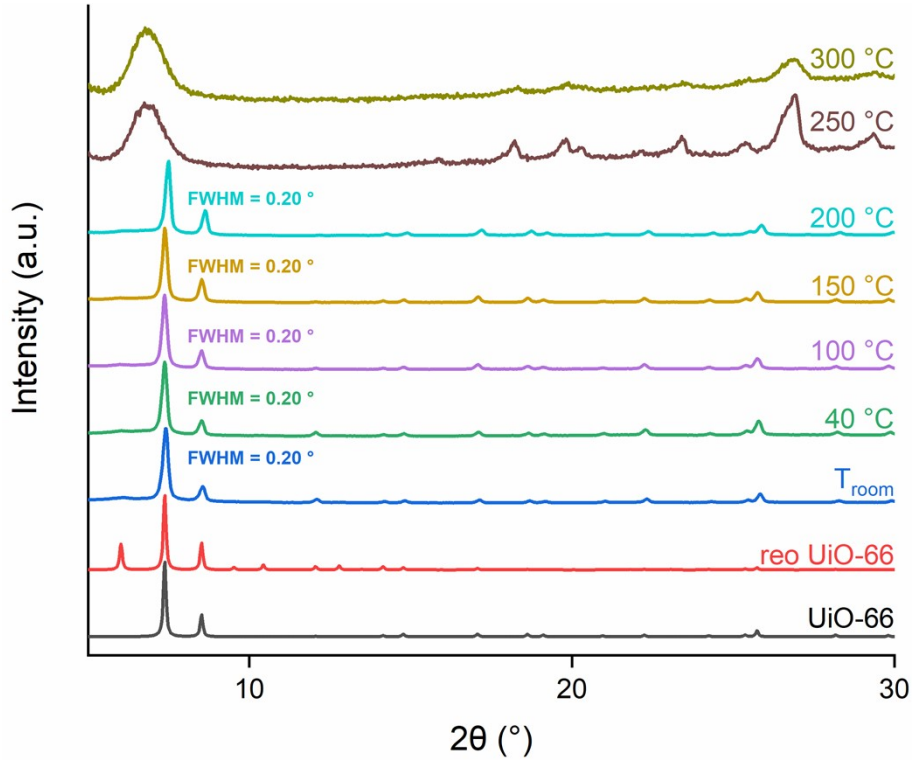

Figure S36: VT-PXRD patterns of P39_LS from room temperature (T_{room}) to 300 °C.